ACS APPLIED MATERIALS & INTERFACES

Letter

www.acsami.org

Optimization of $Zn_xFe_{3-x}O_4$ Hollow Spheres for Enhanced Microwave Attenuation

Zhihong Yang,[†,‡] Zhengwen Li,[†] Yanhui Yang,*[,‡] and Zhichuan J. Xu*[,§]

[†]Temasek Laboratories, National University of Singapore, 5A Engineering Drive 1, Singapore 117411

[‡]School of Chemical and Biomedical Engineering, Nanyang Technological University, Singapore 637459

[§]School of Materials Science and Engineering, Nanyang Technological University, Singapore 639798

Supporting Information

ABSTRACT: We report here the composition optimization of $Zn_xFe_{3-x}O_4$ hollow nanospheres for enhancing microwave attenuation. $Zn_xFe_{3-x}O_4$ hollow nanospheres were synthesized through a simple solvothermal process. The maximum magnetization moment of 91.9 emu/g can be obtained at x = 0.6. The composite filled with $Zn_{0.6}Fe_{2.4}O_4$ exhibited the bandwidth of 3.21−8.33 GHz for RL < −10 dB and a maximum relative bandwidth ($W_{p,max}$) of 88.6% at optimized thickness t_0 = 0.34 cm. The enhancement should be attributed to the enhanced permeability resonance at high frequency. This optimized hollow material is very promising to be used as a mass efficient and broadband microwave attenuation material.

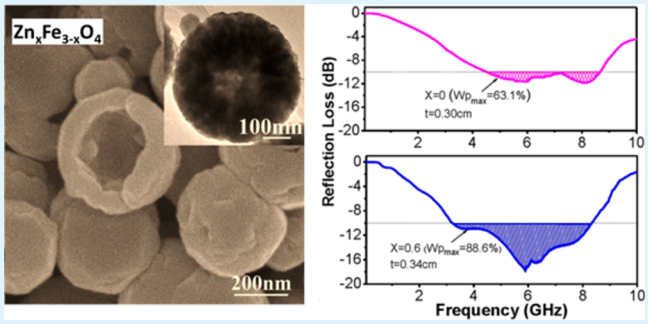

KEYWORDS: *hollow spheres, magnetic materials, solvothermal process, microwave attenuation*

With the rapid development and extensive utilization of mobile electronic devices, the electromagnetic interference (EMI) has become a problem in recent years affecting the living and working environment. To reduce the influence of EMI to certain locations, unwanted electromagnetic waves should be shielded. The electromagnetic wave attenuation (EMA) materials with the capability of shielding desired electromagnetic signals are particularly interesting to this purpose. To date, the most popular EMA materials include carbon-based materials,[1,2] magnetic metals,[3−5] ferrites,[6,7] and conducting polymers and foams.[8,9] Among these EMA materials, the ferrites have the relative better permittivity and permeability properties, which result in the better impedance matching and thus the broad bandwidth. During the past decade, spinel ferrite nanoparticles have attracted intensive attention because they exhibit some distinct magnetic properties compared to bulk counterparts and this allowed further fine-tuning of the EMA material characteristics.[10,11] For examples, Fe_3O_4 nanoparticle composites synthesized by a simple hydrothermal method exhibited a maximum reflection loss of −21.2 dB at 8.16 GHz.[12] $NiFe_2O_4$ nanoparticles synthesized by the polyacrylamide gel method and this ferrite showed a maximum reflection loss of −13 dB at 11.5 GHz with a −10 dB bandwidth over the frequency range of 10.3−13 GHz.[13] It should be noticed that these ferrites have to be filled into the EMA composites with a high content to achieve a high reflection loss and a wide −10 dB bandwidth. It lowers the overall mass efficiency of EMA composite and restricts the use of ferrite nanoparticles in practical applications. One rational way to overcome this shortcoming is to lower the density of these materials by making them hollow and/or porous. The low density forms enable them to be filled into the EMA composite with a higher mass efficiency. To date, the studies of hollow/porous ferrite particles for the application in microwave attenuation were very limited. Recently, it has been reported that the synthesis of hollow magnetite nanospheres and using them as fillers to prepare the EMA composites.[14] The results showed the good refection loss (RL) value at certain frequency range, but the bandwidth with the RL value < −10 dB is still very narrow. According to the Landau-Lifshitz−Gilbert (LLG) equation,[15] the key material parameters which determine the dynamic magnetic properties of the soft ferromagnetic materials are the magnetic anisotropy and saturation magnetization. Therefore, in orderto achieve better microwave properties, the higher saturation magnetization value (M_s) is necessary. In addition, because of the coexistence of Fe^{2+} and Fe^{3+} ions in magnetite, the electron transfer between these two ions would increase the permittivity value and result in the poor impedance match.[16] Therefore, here we demonstrate a strategy to improve the EMA properties for the hollow magnetite by partly substitution of Fe atoms with Zn atoms. The x value of $Zn_xFe_{3-x}O_4$ was optimized to achieve the best performance. The attenuation performance shows the enhanced microwave

Received: October 31, 2014
Accepted: December 11, 2014
Published: December 11, 2014

attenuation and a wide bandwidth (RL < −10 dB) as compare to pure magnetite. It is expected that this $Zn_xFe_{3-x}O_4$ hollow nanosphere can be used as a mass efficient EM attenuation filler for a wide GHz range.

Figure 1 shows representative SEM and TEM images of as-synthesized $Zn_xFe_{3-x}O_4$ (here x = 0.6). It shows that as-synthesized $Zn_xFe_{3-x}O_4$ is spherical with an average diameter of 400 nm. The inset in Figure 1a shows the histogram of the particle size distribution. The SEM and TEM images of as-synthesized $Zn_xFe_{3-x}O_4$ (here x = 0, 0.2, 0.4, and 0.8) are shown in Figure S1 in the Supporting Information. It shows that the morphology and particle size remained unchanged as the composition varies. Figure 1b shows a broken sphere. It indicates that the spheres are hollow interior and the wall thickness is around 100 nm. The hollow structure is further confirmed by TEM (shown in the inset of Figure 1b). The intensive contrast between the black margin and the bright center of the particles confirms the existence of hollow structures in the resulting spheres. More detailed information on the synthesized $Zn_xFe_{3-x}O_4$ hollow spheres were also investigated through the high-resolution TEM (HRTEM) analysis which is shown in the Supporting Information (Figure S2). All the prepared hollow Fe_3O_4 nanospheres with different amounts of Zn doping can be confirmed to the cubic-structured spinel phase (JCPDS No. 85−1436) through the XRD analysis (Figure S3 in the Supporting Information). The actual ratios of Zn to Fe of as-prepared $Zn_xFe_{3-x}O_4$ nanospheres were determined by EDS (shown in Figure S4 in the Supporting Infomration). The composition of each sample was obtained by averaging at least six measurements in different areas and under different magnifications. The result confirmed that the ratios of Zn and Fe are maintained as the feeding ratios of Zn and Fe precursors. Figure S5 in the Supporting Information shows the Raman spectra of $Zn_xFe_{3-x}O_4$ samples with x = 0 and 0.6 at room temperature and the recorded range is from 200 to 800 cm^{-1}. In this region, the cubic AB_2O_4 spinel structure shows five active Raman modes (A_{1g} + E_g+3T_{2g}). It is generally accepted that the modes above 600 cm^{-1} can be assigned to the A_{1g} symmetry, which is related to motions of O in tetrahedral AO4 groups.[17] For the x = 0 sample, the single peak at ∼690 cm^{-1} should be due to the corresponding oxygen vibrations against iron. For the x = 0.6 sample, the split A_{1g} mode indicates the coexistence of two AO_4 groups, A being either Zn or Fe. According to the previous study,[18] the Raman mode peaking at ∼650 cm^{-1} is attributed to the oxygen breathing vibrations against zinc. Thus, it is clear that the zinc ion have been incorporated into the spinel ferrite.

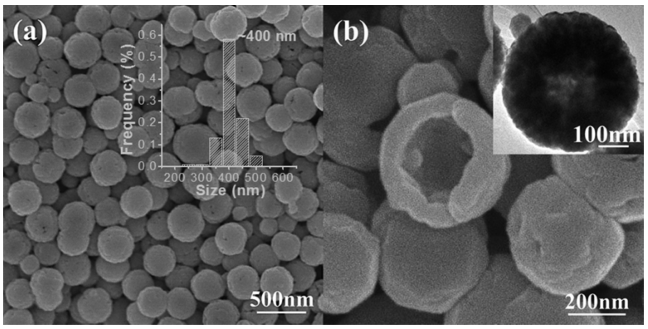

Figure 1. (a) Low-magnification and (b) high-magnification SEM images of the $Zn_xFe_{3-x}O_4$ hollow nanospheres (x = 0.6). The inset of a is particle size distribution and the inset of b is a TEM image of a $Zn_xFe_{3-x}O_4$ hollow nanosphere (x = 0.6).

Figure 2a and b shows the magnetization hysteresis curves of $Zn_xFe_{3-x}O_4$ spheres at room temperature and the Saturation magnetization (M_s) and Coercivity (H_c) values as a function of Zn substitution amounts (x), respectively. It is clearly shown that both M_s and H_c are strongly dependent on the doping amounts of Zn ion (x). With increasing Zn content from x = 0 to 0.6, the M_s value increases from 84.5 to 91.9 emu/g and when the Zn content further increases to x = 0.8, the M_s value sharply decreases to 77.7, which is even lower than the prepared Fe_3O_4 samples without Zn doping. The initial increase in M_s with increasing Zn content may be attributed to the cation distribution among A and B-sites in the spinel structure. For spinel ferrite, the origin of net moment in a unit formula is from the arithmetic difference between the magnetic moments at A-sites (upward) and at B-sites (downward).[19] Because the nonmagnetic Zn^{2+} ion which preferentially occupies A-site[20] will replace the magnetic Fe^{3+} ions in A-site. The increase in the net magnetization between A- and B-sites (up to x = 0.6) results in the increased M_s value. The decrease in M_s for x > 0.6 may be associated with a change for the dominant super-exchange interaction from A−O-B (exchange interaction between the magnetic moments at the A and B sites) to B−O−B (exchange interaction between the magnetic moments at B sites). At a certain critical doping level (x = 0.6 in this case), the B−O−B superexchange interaction becomes dominant and it is well-known that in spinel ferrites, the A−O−B exchange interaction is much stronger than the B−O−B and the A−O−A

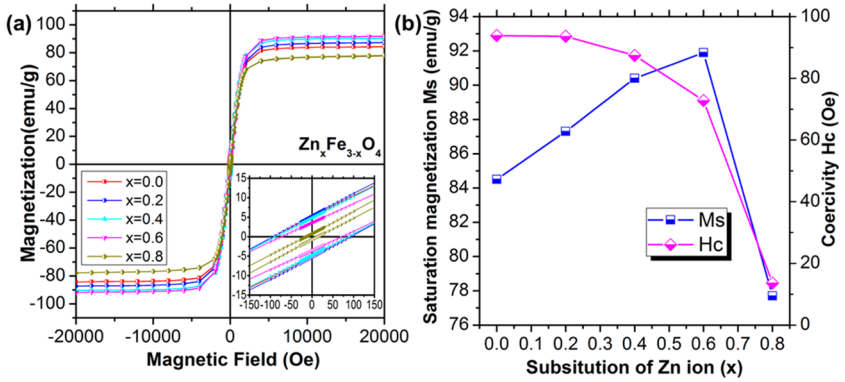

Figure 2. (a) Hysteresis loops of $Zn_xFe_{3-x}O_4$ hollow nanospheres measured at room temperature. (b) Dependences of Saturation magnetization (M_s) and Coercivity (H_c) on the Zn substitution content (x).

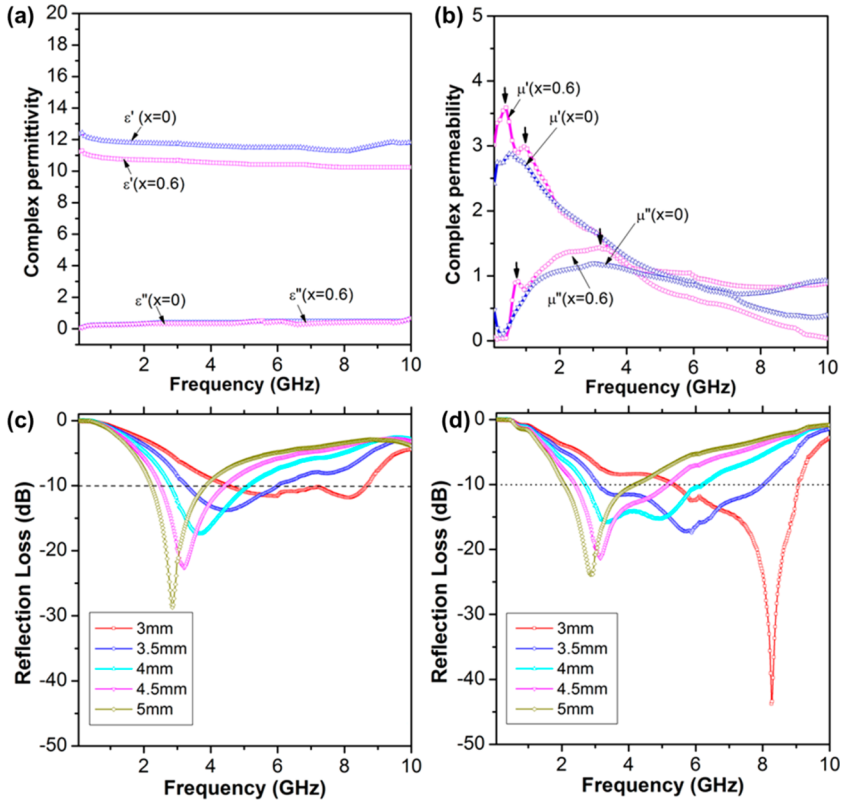

Figure 3. (a, b) Complex permittivity and permeability curves of the silicon resin composites filled with 35 vol % of hollow magnetite and $Zn_{0.6}Fe_{2.4}O_4$ nanospheres and (c, d) the calculated reflection loss (RL) for these two composites.

interactions,[21] thus the change from A−O−B to B−O−B superexchange interactions will cause the rapidly decrease in the total magnetic moment. Meanwhile, the H_c value decreases slightly with increasing Zn^{2+} content up to $x = 0.6$, whereas it gives a sharp decrease with further increasing the Zn^{2+} content to 0.8. The decrease in H_c should be attributed to the weakened A−O−B superexchange interaction when the Zn^{2+} doping amount is below $x = 0.6$. And the sharply decrease after the doping amount of $x = 0.6$ is also due to the change from A−O−B to B−O−B superexchange interaction.

According to the Globus equation $\mu_i' \propto (M_s^2 D/(K_1)^{1/2})$, the higher saturation magnetization (M_s), larger grain size (D), and lower magnetocrystalline anisotropy constant (K_1) may contribute a higher complex permeability. On the basis of the static magnetic results, $Zn_xFe_{3-x}O_4$ spheres with $x = 0$ and 0.6 (highest M_s value) were chosen as the filler to mix with silicon resin for microwave measurement. The acquired electromagnetic parameters (ε', ε'', μ', and μ'') of as-measured samples in the frequency range of 0.05 to10 GHz are shown in Figure 3a, b. For both of composites, the relative permittivity (ε', ε'') are almost constant in the whole frequency range. The ε' and ε'' values of the $x = 0$ composites are around 12.3 and 0.05, respectively. And a slightly decrease in the ε' value can be found for the composites with the Zn doping amount of $x = 0.6$. This slightly decrease can be understood by the reduction the amount of Fe^{2+} ions after the substitution of Zn^{2+} ions according to the expressed chemical composition of $Zn^{2+}{}_xFe^{3+}{}_{A(1-x)}Fe^{3+}{}_{B(1+x)}Fe^{2+}{}_{B(1-x)}O^{2-}{}_4$.[22] In that way, the electron transfer between Fe^{3+} and Fe^{2+} can be depressed, which results in the lower permittivity value. The permeability spectra in Figure 3b show the obviously different trends for these two kinds of composites. For the $x = 0$ composites, a single resonance peak can be observed. The μ' value decreases sharply when the frequency is above 1 GHz. Meanwhile, the μ'' starts to increase, then reaches a maximum value of 1.21 at 3.05 GHz and finally decreases slowly to almost 0.5 at 10 GHz. For the $x = 0.6$ composites, two obviously resonance peaks exist in the measured frequency range. Two peaks of the imaginary part of permeability appear at 0.75 and 3.18 GHz and the maximum μ'' value is about 1.43, which is higher than $x = 0$ composites. The mechanism for the appearance of these two resonance peaks after Zn doping could not be well understood at this moment. Possible explanations are as follows: According to the Srivastava's theory,[23] the permeability spectrum is related to domain structures. The resonance peak at low frequency (<1 GHz) should attribute to the domain wall resonance. The resonance peak at high frequency (>1 GHz) should attribute to the nature resonance. Due to a higher magnetocrystalline anisotropy (K_1) for Fe_3O_4 $(x = 0)$ samples, the domain wall resonance may be restrained. However, after Zn doping, the magnetocrystalline anisotropy (K_1) will be decreased, which may recover the appearance of domain wall resonance. Further investigations need to be done to confirm this possible mechanism in future.

Figure 3c, d shows the calculated dependence of reflection loss (RL) on frequency with various thickness t for the silicon resin composites with 65 wt % Fe_3O_4 $(x = 0)$ and $Zn_{0.6}Fe_{2.4}O_4$ $(x = 0.6)$ hollow spheres, respectively. It is clearly shown that at the same thickness, the $Zn_{0.6}Fe_{2.4}O_4$ composites have lower reflection loss and broader bandwidth for RL < −10 dB as compared to the pure Fe_3O_4 composites. Another important parameter is the frequency band of EM attenuation composites. In general, percentage bandwidth, W_p, is defined as $(f_{up} - f_{low})/f_0 \times 100\%$ where f_{up} and f_{low} are the frequency upper and lower

dx.doi.org/10.1021/am5075612 | ACS Appl. Mater. Interfaces 2014, 6, 21911−21915

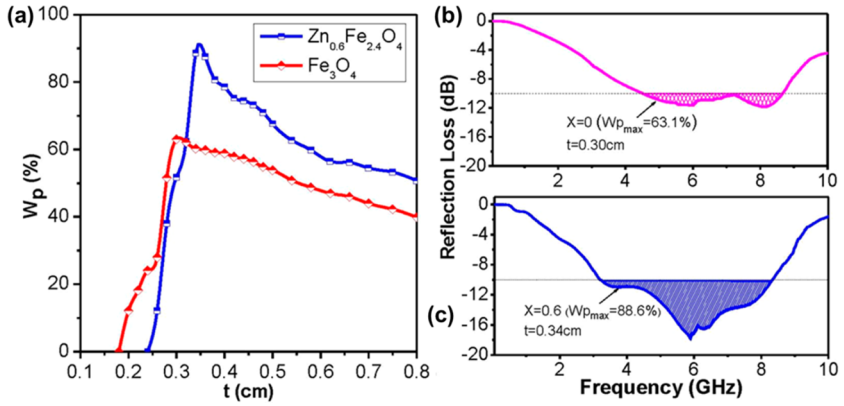

Figure 4. (a) Dependence of percentage bandwidth W_p on thickness t for composites with hollow magnetite and $Zn_{0.6}Fe_{2.4}O_4$ nanospheres as fillers and (b, c) the predicted RL-f curves at optimum thickness for $Zn_xFe_{3-x}O_4$ hollow spheres with (b) x = 0 and (c) 0.6.

limits of the bandwidth for a give reflection loss (such as RL < −10 dB) and f_0 is the center frequency for the bandwidth.[24] Figure 4a shows the dependence of the percentage bandwidth W_p for RL < −10 dB on the thickness t, which is obtained from the corresponding RL−f curve. For both of composites, with increasing the thickness t from 0.1 to 0.8 cm, W_p rapidly increase at first to reach the maximum and then slowly decreases. Commonly, the maximum W_p is marked with $W_{p,max}$ and the corresponding thickness is known as the optimum thickness. Figure 4b, c show the RL−f curves at to for these two kinds of composites. For x = 0 composites, the frequency band for RL < −10 dB is from 4.51 to 8.66 GHz and $W_{p,max}$ is about 63.1% at the optimum thickness of t_o = 0.30 cm. But for x = 0.6 composites, the band for RL < −10 dB is from 3.21 to 8.33 GHz and a maximum relative bandwidth $W_{p,max}$ of 88.6% is achieved at t_o = 0.34 cm. The $W_{p,max}$ for the x = 0.6 composites is expanded by 25.5%, as compared to the x = 0 composites. Meanwhile, the x = 0.6 composites also show the enhanced RL value of −18 dB, which is lower than −12 dB for the x = 0 composites. It is well-known that two key factors that determine the RL values and the bandwidth: (1) the incident microwave that can transmit into the materials with minimum reflection and (2) the materials that can effectively attenuate the microwave transmitted into the composites.To allow the incident microwave transmit into the materials instead of reflecting back to the space, the material should have an impedance matching with that of free space, i.e., the material should have close values of permittivity and permeability. To achieve effective attenuation, the high magnetic/dielectric loss is required.[16,25] In our case, the decrease in complex permittivity and the increase in complex permeability lead to the closer values of the two and thus a better impedance matching. The increased magnetic loss results in a better attenuation. Thus, the enhanced RL and broader bandwidth should be attributed to the increased complex permeability and decreased complex permittivity for the Zn-doped Fe_3O_4 samples. Therefore, $Zn_xFe_{3-x}O_4$ hollow spheres obtained in this work are attractive candidates for lightweight and broadband microwave attenuation materials.

In summary, we optimized the composition of $Zn_xFe_{3-x}O_4$ hollow spheres for enhancing electromagnetic wave attenuation. With increasing the Zn amount from x = 0 to x = 0.8, the M_s value increases at first and then dramatically decreases, the maximum value of 91.9 emu/g can be obtained at Zn content of x = 0.6. As compared to the Fe_3O_4 samples without ZnO doping, the composites filled with Zn content of x = 0.6 samples shows the enhanced reflection loss and broader bandwidth for RL < −10 dB. The bandwidth for RL < −10 dB can cover from 3.21 to 8.33 GHz and a maximum relative bandwidth ($W_{p,max}$) of 88.6% is achieved at optimal thickness t_o = 0.34 cm. It is expected that this optimized hollow materials can be used as a mass efficient and broadband microwave attenuation materials.

■ ASSOCIATED CONTENT

Supporting Information

Experimental details, SEM and TEM images of the $Zn_xFe_{3-x}O_4$ hollow nanospheres, SAED pattern and HRTEM image of the $Zn_xFe_{3-x}O_4$ (x = 0.6) hollow nanospheres, XRD patterns of obtained hollow magnetite nanospheres with different Zn substitution, EDS spectra and measured compositions of the $Zn_xFe_{3-x}O_4$ hollow nanospheres, and Raman spectra of the $Zn_xFe_{3-x}O_4$ hollow nanospheres. This material is available free of charge via the Internet at http://pubs.acs.org/.

■ AUTHOR INFORMATION

Corresponding Authors

* E-mail: xuzc@ntu.edu.sg.
*E-mail: yhyang@ntu.edu.sg

Notes

The authors declare no competing financial interest.

■ REFERENCES

(1) Cao, M. S.; Yang, J.; Song, W. L.; Zhang, D. Q.; Wen, B.; Jin, H. B.; Hou, Z. L.; Yuan, J. Ferroferric Oxide/Multiwalled Carbon Nanotube vs Polyaniline/Ferroferric Oxide/Multiwalled Carbon Nanotube Multiheterostructures for Highly Effective Microwave Absorption. *ACS Appl. Mater. Interfaces* **2012**, *4*, 6949−6956.

(2) Ren, Y. L.; Wu, H. Y.; Lu, M. M.; Chen, Y. J.; Zhu, C. L.; Gao, P.; Cao, M. S.; Li, C. Y.; Ouyang, Q. Y. Quaternary Nanocomposites Consisting of Graphene, Fe_3O_4@Fe Core@Shell, and ZnO Nanoparticles: Synthesis and Excellent Electromagnetic Absorption Properties. *ACS Appl. Mater. Interfaces* **2012**, *4*, 6436−6442.

(3) Shi, X. L.; Cao, M. S.; Yuan, J.; Fang, X. Y. Dual Nonlinear Dielectric Resonance and Nesting Microwave Absorption Peaks of Hollow Cobalt Nanochains Composites with Negative Permeability. *Appl. Phys. Lett.* **2009**, *95*, 163108.

(4) Yang, Z. H.; Li, Z. W.; Yu, L. H.; Yang, Y. H.; Xu, Z. C. Achieving High Performance Electromagnetic Wave Attenuation: A Rational Design of Silica Coated Mesoporous Iron Microcubes. *J. Mater. Chem. C* **2014**, *2*, 7583−7588.

(5) Yang, Y.; Xu, C. L.; Xia, Y. X.; Wang, T.; Li, F. S. Synthesis and Microwave Absorption Properties of FeCo Nanoplates. *J. Alloys Compd.* **2010**, *493*, 549−552.
(6) Yang, Z. H.; Li, Z. W.; Liu, L.; Kong, L. B. Enhanced Microwave Magnetic and Attenuation properties of Composites with Free-Standing Spinel Ferrite Thick Films as Fillers. *J. Magn. Magn. Mater.* **2012**, *324*, 3144−3148.
(7) Meshram, M. R.; Agrawal, N. K.; Sinha, B.; Misra, P. S. Characterization of M-type Barium Hexagonal Ferrite-based Wide Band Microwave absorber. *J. Magn. Magn. Mater.* **2004**, *271*, 207−214.
(8) Lakshmi, K.; John, H.; Mathew, K. T.; Josepha, R.; George, K. E. Microwave Absorption, Reflection and EMI shielding of PU−PANI Composite. *Acta Mater.* **2009**, *57*, 371−375.
(9) He, Y. F.; Gong, R. Z. Preparation and Microwave Absorption Properties of Foam-based Honeycomb Sandwich structures. *EPL* **2009**, *85*, 58003.
(10) Kodama, R. H. Magnetic Nanoparticles. *J. Magn. Magn. Mater.* **1999**, *200*, 359−372.
(11) Batlle, X.; Labarta, A. Finite-size Effects in Fine Particles: Magnetic and Transport Properties. *J. Phys. D: Appl. Phys.* **2002**, *35*, R15−R42.
(12) Ni, S. B.; Lin, S. M.; Pan, Q. T.; Yang, F.; Huang, K.; He, D. Y. Hydrothermal Synthesis and Microwave Absorption Properties of Fe_3O_4 Nanocrystals. *J. Phys. D: Appl. Phys.* **2009**, *42*, 055004.
(13) Zhao, H. T.; Sun, X. D.; Mao, C. H.; Du, J. Preparation and Microwave−Absorbing Properties of $NiFe_2O_4$-Polystyrene Composites. *Phys. B: Condensed Matter* **2009**, *404*, 69−72.
(14) Wang, F. L.; Liu, J. R.; Kong, J.; Zhang, Z. J.; Wang, X. Z.; Itoh, M.; Machida, K. I. Template Free Synthesis and Electromagnetic Wave Absorption Properties of Monodispersed Hollow Magnetite nanospheres. *J. Mater. Chem.* **2011**, *21*, 4314−4320.
(15) Gilbert, T. L. A Phenomenological Theory of Damping in Ferromagnetic Materials. *IEEE Trans. Magn.* **2004**, *40*, 3443−3449.
(16) Yan, L. G.; Wang, J. B.; Han, X. H.; Ren, Y.; Liu, Q. F.; Li, F. S. Enhanced Microwave Absorption of Fe Nanoflakes after Coating with SiO_2 Nanoshell. *Nanotechnology* **2010**, *21*, 095708.
(17) Silva, S. W.; Nakagomi, F.; Silva, M. S.; Franco, A.; Garg, V. K.; Oliveira, A. C.; Morais, P. C. Effect of the Zn Content in the Structural and Magnetic properties of $Zn_xMg_{1-x}Fe_2O_4$ mixed Ferrites monitored by Raman and Mössbauer Spectroscopies. *J. Appl. Phys.* **2010**, *107*, 09B503.
(18) Maletin, M.; Moshopoulou, E. G.; Kontos, A. G.; Devlin, E.; Delimitis, A.; Zaspalis, V. T.; Nalbandian, L.; Srdic, V. V. Synthesis and Structural Characterization of In-doped $ZnFe_2O_4$ nanoparticles. *J. Eur. Ceram. Soc.* **2007**, *27*, 4391−4394.
(19) Yang, Y.; Liu, X. L.; Yang, Y.; Xiao, W.; Li, Z. W.; Xue, D. S.; Li, F. S.; Ding, J. Synthesis of Nonstoichiometric Zinc Ferrite Nanoparticles with Extraordinary room temperature Magnetism and their diverse Applications. *J. Mater. Chem. C* **2013**, *1*, 2875−2885.
(20) Takaobushi, J.; Tanaka, H.; Kawai, T.; Ueda, S.; Kim, J.; Kobata, K.; Ikenaga, E.; Yabashi, M.; Kobayashi, K.; Nishino, Y.; Miwa, D.; Tamasaku, K.; Ishikawa, T. $Fe_{3-x}Zn_xO_4$ Thin film as Tunable High Curie temperature Ferromagnetic Semiconductor. *Appl. Phys. Lett.* **2006**, *89*, 242507.
(21) Ligenza, S. A Study of the $^6S_{5/2}$-Term Splitting of an Fe^{3+} Ion in Zinc Ferrite by Neutron Spectroscopy. *Phys. Status Solidi B* **1976**, *75*, 315−326.
(22) Cheng, Y. H.; Li, L. Y.; Wang, W. H.; Liu, H.; Ren, S. W.; Cui, X. Y.; Zheng, R. K. Tunable Electrical and Magnetic properties of Half-Metallic $Zn_{(x)}Fe_{(3-x)}O_4$ from first Principles. *Phys. Chem. Chem. Phys.* **2011**, *13*, 21243−7.
(23) Srivastava, C. M.; Shringi, S. N.; Srivastava, R. G.; Nandikar, N. G. Mössbauer study of Relaxation Phenomena in Zinc-ferrous Ferrites. *Phys. Rev. B: Solid State* **1976**, *14*, 2032−2041.
(24) Li, Z. W.; Yang, Z. H.; Kong, L. B. Enhanced Microwave Magnetic and Attenuation properties for Z-type Barium ferrite Composites with Flaky Fillers. *J. Appl. Phys.* **2011**, *110*, 063907.
(25) Yang, Z. H.; Li, Z. W.; Yang, Y. H.; Liu, L.; Kong, L. B. Dielectric and Magnetic Properties of NiCuZn Ferrite coated Sendust Flakes through a Sol−Gel Approach. *J. Magn. Magn. Mater.* **2013**, *331*, 232−236.